
IPDreamer: Appearance-Controllable 3D Object Generation with Complex Image Prompts

Bohan Zeng^{1*}, Shanglin Li^{1*}, Yutang Feng^{1*}, Ling Yang^{5†}, Hong Li¹
Sicheng Gao¹, Jiaming Liu³, Conghui He⁷, Wentao Zhang⁵, Jianzhuang Liu²
Baochang Zhang^{1,4†}, Shuicheng Yan⁶

¹Institute of Artificial Intelligence, Beihang University

²Shenzhen Institute of Advanced Technology, Shenzhen, China

³Tiamat AI ⁴Zhongguancun Laboratory, Beijing, China

⁵Peking University ⁶Skywork AI

⁷Shanghai Artificial Intelligence Laboratory

Abstract

Recent advances in 3D generation have been remarkable, with methods such as DreamFusion leveraging large-scale text-to-image diffusion-based models to supervise 3D object generation. These methods enable the synthesis of detailed and photorealistic textured objects. However, the appearance of 3D objects produced by these text-to-3D models is unpredictable, and it is hard for the single-image-to-3D methods to deal with complex images, thus posing a challenge in generating appearance-controllable 3D objects. To achieve controllable complex 3D object synthesis, we propose IPDreamer, a novel approach that incorporates Image Prompt adaption to extract detailed and comprehensive appearance features from complex images, which are then utilized for 3D object generation. Our results demonstrate that IPDreamer effectively generates high-quality 3D objects that are consistent with both the provided text and the appearance of complex image prompts, demonstrating its promising capability in appearance-controllable 3D object generation. Our code is available at <https://github.com/zengbohan0217/IPDreamer>.

1 Introduction

The rapid evolution of 3D technology has revolutionized the way we create and interact with virtual worlds. 3D technology is now essential in a wide range of fields, including architecture, gaming, mechanical manufacturing, and AR/VR. However, creating high-quality 3D content remains a challenging and time-consuming task, even for experts. To address this challenge, researchers have developed text-to-3D methodologies that automate the process of generating 3D assets from textual descriptions. Built on the 3D scene representation capabilities of Neural Radiance Fields (NeRFs) [39, 43] and the rich visual prior knowledge of pretrained diffusion models [56, 57], recent research [23, 40, 50, 31, 7, 74] has made significant progress, simplifying the text-to-3D pipeline and making it more accessible, which causes a significant shift in these fields.

Recent advances in diffusion models have significantly enhanced the capabilities of text-to-image generation. State-of-the-art (SOTA) systems, leveraging cutting-edge diffusion-based techniques [46, 56, 2, 81, 21], can now generate and modify images directly from textual descriptions with vastly improved quality and controllability. Inspired by the rapid development of text-to-image generation, recent works [50, 31, 7] utilize pretrained text-to-image diffusion models and the Score Distillation

*These authors contributed equally.

†Corresponding Author: bczhang@buaa.edu.cn, yangling0818@163.com.

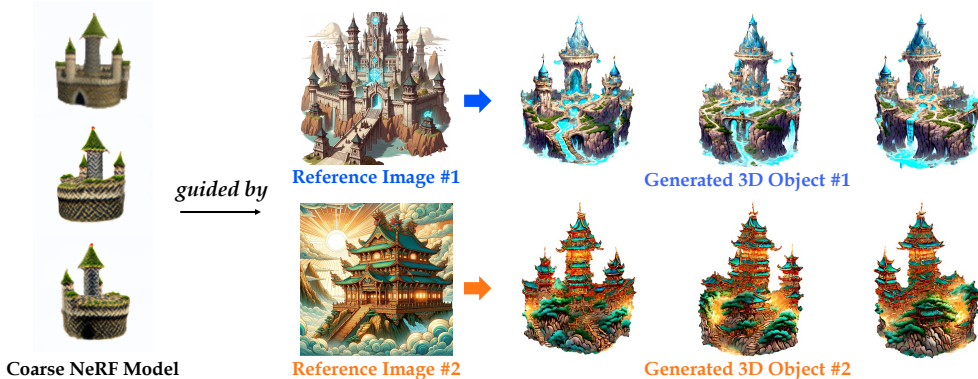


Figure 1: IPDREAMER can generate controllable, desired, and high-quality 3D objects based on given textual and image prompts. The figure illustrates two high-quality 3D objects with rich details, which are initialized by the same NeRF model and guided by different complex reference image prompts.

Sampling (SDS) algorithm to optimize 3D representations. The rendering results of these optimized representations are more photo-realistic than those optimized by CLIP models [40, 23].

To address the over-smoothing and low-diversity problems of SDS, ProlificDreamer [74] proposes Variational Score Distillation (VSD) for high-quality and more diverse 3D scene and object synthesis. However, The appearance of its generated results is uncontrollable due to the randomness in the training process of the Low-Rank Adaptation model [21] adopted in VSD.

Unlike the unpredictability in text-to-3D generation, single-image-to-3D generation allows for strict control over the appearance of the generated 3D results. However, existing single-image-to-3D methods [34, 35, 60] are limited to handling simple images containing clearly defined objects, often struggling with complex images, which are characterized by rich content, intricate composition, and lack of a clear subject. For example, they cannot deal with the complex images provided in Fig. 1.

To achieve controllable high-quality 3D object generation guided by complex images, we propose *IPDREAMER*, a novel approach that incorporates image prompt adaption to provide specific and comprehensive appearance³ information for 3D generation.

Recently, some methods [79, 82, 72] use image prompts to modify the cross attention in diffusion models for better control of image generation. In this paper, we extend SDS to *Image Prompt Score Distillation* (IPSD), which leverages image prompts to guide the optimization of 3D object appearance. With IPSD, IPDREAMER can utilize a complex image to obtain appearance-controllable and high-quality 3D object generation.

Specifically, our IPDREAMER initiates the process by creating coarse NeRF models [39] which can be guided by textual prompts or simple images. Next, we generate 2D complex guidance images, the characteristics of which can be selected or controlled by the user. Finally, we employ the image prompt encoder from [79] to extract image prompt features from provided 2D images and their corresponding normal maps and utilize these features to guide the optimization of the texture and geometry of the 3D meshes, respectively. Besides, we propose a scheme named Local Editing with Partial Images (LEPI) to generate desirable 3D objects when the appearance of the provided image prompt significantly deviates from the initial coarse NeRF model.

As illustrated in Fig. 1, IPDREAMER can transfer the appearances of complex reference images to the NeRF model and generate high-quality 3D objects, which also demonstrates the efficacy of using image prompts for guiding texture optimization.

In summary, the main contributions of this paper are as follows:

- We present IPDREAMER, a novel 3D object synthesis framework that enables users to create controllable, high-quality 3D objects effortlessly. Compared with previous methods, IP-

³In this paper, the appearance of an object/scene includes its shape, texture, and color.

Dreamer excels in synthesizing a high-quality 3D object whose style aligns with a provided complex image prompt.

- We introduce Image Prompt Score Distillation (IPSD), which utilizes image prompt adaption to guide 3D mesh generation and provides substantial appearance information.
- We propose Local Editing with Partial Images (LEPI) to generate desirable 3D objects when the initial NeRF models significantly differ from the provided image prompts.
- Comprehensive experiments demonstrate that IPDreamer achieves high-quality 3D generation and excellent rendering results, outperforming existing SOTA methods.

2 Related Work

2.1 Diffusion Models

Diffusion models (DMs) are originally introduced as a generative model for gradually denoising images corrupted by Gaussian noise to generate samples [61]. Recent advancements in DMs [19, 62, 9, 71, 56, 48] have shown their exceptional performance in image synthesis. DMs have also achieved state-of-the-art results in various synthesis tasks, including text-to-image generation [57, 46, 54, 49, 78], inpainting [1, 36, 79], 3D object synthesis [29, 37], video synthesis [20, 18], speech synthesis [26, 32], super-resolution [28, 58, 11], face animation [51], text-to-motion generation [67], and brain signal visualization [63, 64]. Some DMs [27, 73] can produce diverse results by learning the internal patch distribution from a single image. [41, 70, 75, 12] enhance image/video editing with pre-trained DMs in a zero-shot or one-shot manner. These advancements highlight the versatility and potential of DMs across a wide range of synthesis applications.

2.2 Controllable Generation and Editing

Controllable generation and editing of 2D images and 3D objects are core goals of generative tasks. With the emergence of large language models (LLMs) such as GPT-3 and Llama [3, 68, 69], instruction-based user-friendly generative control has gained much attention. InstructPix2Pix [2] and MagicBrush [80] build datasets based on LLMs and large text-to-image models to achieve effective instruction control on 2D images. InstructNeRF2NeRF [15] combines this method with NeRF scene reconstruction [39] to introduce instruction control into 3D generation. Meanwhile, a series of adapter methods such as ControlNet and IP-Adapter [81, 21, 42, 84, 79, 22] provide reliable approaches for fine-tuning large pre-trained DMs (e.g., Stable Diffusion [56] and Imagen [57]) for conditional controllable generation (e.g., using sketch, canny, pose, etc. to control image structure). Among them, IP-Adapter [79] introduces a decoupled cross-attention mechanism to achieve effective appearance generation control using image prompts.

2.3 3D Generation

In recent years, 3D generative modeling has attracted a large number of researchers. Inspired by the recent neural volume rendering, many 3D-aware image rendering methods [4, 5, 13, 14, 45, 47] are proposed to generate high-quality rendered 2D images for 3D visualization. Meanwhile, with the development of text-to-image synthesis, researchers have shown a growing interest in text-to-3D generation. Early methods such as DreamField [23] and CLIPmesh [40] achieve text-to-3D generation by utilizing a pretrained image-text aligned model CLIP [53]. They optimize the underlying 3D representations (NeRFs and meshes) to ensure that all 2D renderings have high text-image alignment scores. Recently, [50, 31, 7, 74, 6] have achieved high-quality 3D synthesis (NeRFs and meshes) by leveraging a robust pretrained text-to-image DM as a strong prior to guide the training of the 3D model. Other works [60, 83, 34] introduce multi-view DMs to enhance 3D consistency and provide strong structured semantic priors for 3D synthesis. IT3D [8] combines SDS and GAN to refine the 3D model and obtain high-quality 3D synthesis. [65, 30] combine 3D Gaussians [24] with SDS-based optimization to improve 3D synthesis and reduce generation time. Additionally, [38, 66, 33, 52] are capable to generate 3D representations based on single images, and [34, 35, 60, 77] achieve 2D images in multiple viewpoints, which enable consistent 3D object generation. In this work, we introduce IPDreamer, a method that leverages complex image prompts to provide comprehensive appearance information, effectively guiding the synthesis of high-quality 3D objects.

3 Method

In this section, we present the details of IPDreameer. First, we give the problem statement of text-to-3D/single-image-to-3D generation and the preliminaries of SDS. Then, we briefly overview IPDreameer. Finally, we explain the training framework of our two-stage 3D generation, i.e., NeRF training and mesh training.

3.1 Preliminaries

Given a text prompt y or an image I , text-to-3D/single-image-to-3D generation aims at synthesizing novel views and optimizing the parameters of a 3D object/scene that corresponds to the given y or I . DreamFusion [50] utilizes a pretrained text-to-image DM $\epsilon_{pretrain}$ to optimize an MLP parameterized as θ representing a 3D volume, where a differentiable generator g renders θ to create 2D images $x = g(\theta, c)$ given a sampled camera pose c , based on the gradient of the Score Distillation Sampling (SDS) loss:

$$\nabla_{\theta} \mathcal{L}_{SDS}(\theta) = \mathbb{E}_{t, \epsilon} \left[w(t) (\epsilon_{pretrain}(x_t; y, t) - \epsilon) \frac{\partial x}{\partial \theta} \right], \quad (1)$$

where $w(t)$ is a weighting function, $\epsilon_{pretrain}(x_t; y, t)$ predicts the noise $\epsilon \sim \mathcal{N}(0, I)$, given the noisy image x_t , text-prompt features y and timestep t .

Although [31, 7, 74] show excellent text-to-3D generation, the appearances of their 3D synthesis results are uncontrollable. A feasible solution to realize controllable 3D object generation is to use a 2D image as a prior. However, existing single-image-to-3D methods are difficult to obtain high-quality 3D object synthesis from complex single images. To address these problems, we employ the image prompt adaption method [79] to provide sufficient appearance information for 3D object synthesis. Specifically, we first obtain a coarse NeRF model, which can be generated with a pretrained DM (e.g., Stable Diffusion or Zero-1-to-3) with a textual prompt y or an image I_{rgb} . Then we extract the image prompt feature y_{rgb} from I_{rgb} . Based on y_{rgb} , IPDreameer can generate a highly detailed controllable 3D object.

3.2 Overview of IPDreameer

We outline the proposed 3D object generation framework in Fig. 2(a), which has two main stages: NeRF training (Stage 1), and mesh training (Stage 2). The two-stage training aims to generate controllable 3D objects in a coarse-to-fine manner. In Stage 1, we employ NeRF to represent the shape and color of a 3D object, and train a coarse NeRF model that aligns with I_{rgb} which is either provided by the user or generated by a text-to-image model with a textual prompt y . In Stage 2 (Fig. 2(b)), we begin with extracting the 3D mesh from the NeRF using DM Tet [59]. By leveraging the appearance guidance capability of our proposed IPSD for 3D objects, we can replace I_{rgb} used in Stage 1 with another complex image to guide the synthesis of the 3D object. To optimize the geometry of the 3D mesh, we first obtain the normal image I_n from I_{rgb} by DPT [55]. Then we extract another image prompt feature y_n from I_n using the image encoder \mathcal{E}_{image} of the IP adaption method [79]. This y_n is then used by ϵ_{ip} ⁴ in [79] to supervise the generation of the normal image $x_{n,ran}$. To optimize the texture of the 3D mesh, we utilize the image prompt features y_{rgb} and introduce a geometry prompt difference δ_{geo} to supervise the rendering results x_{rgb} of the 3D mesh.

3.3 NeRF Training

Before we optimize the 3D objects by IPSD, we need to obtain a NeRF model which can be either given or generated by a textual prompt y or an image I_{rgb} . In this work, we employ Zero-1-to-3 [34] to train this coarse NeRF model based on the image I_{rgb} generated by the given text prompt y . It is worth noting that obtaining a coarse NeRF model is not the main focus of this work. Leveraging the powerful guidance of IPSD for 3D mesh optimization, simply providing a basic coarse NeRF model is enough. Therefore, besides using Zero-1-2-3 for supervision, alternative methods can also be employed to acquire a coarse NeRF model.

⁴We use ϵ_{ip} to denote the denosing model of the IP adaption method to leverage the image prompt features.

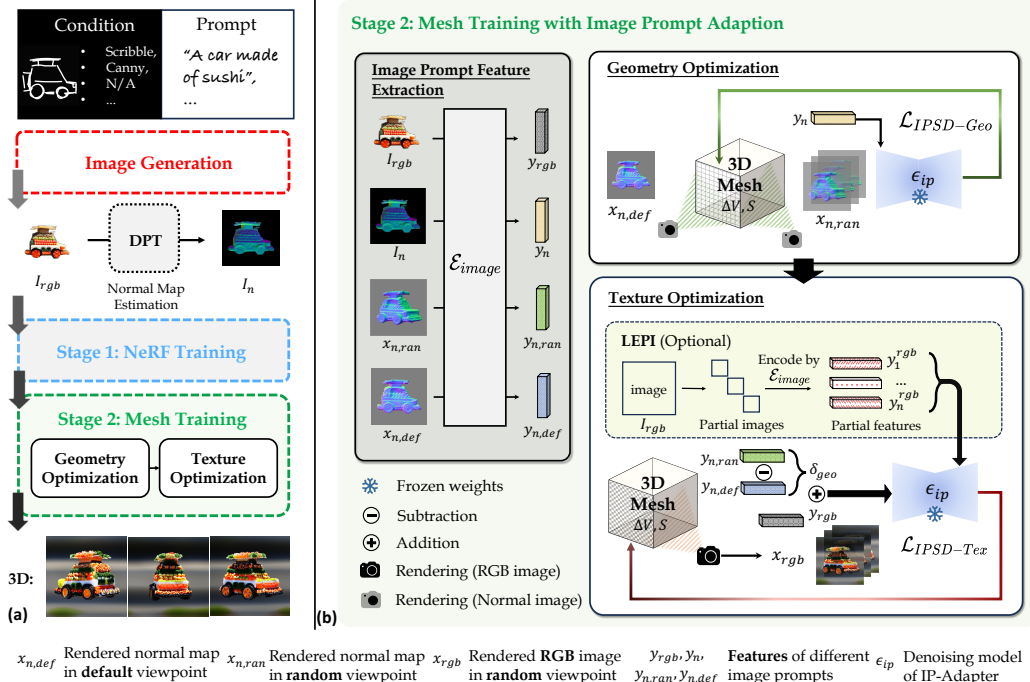


Figure 2: **Overview of IPDREAMER.** IPDREAMER is designed to generate high-quality, controllable 3D objects that align with given textual and/or image prompts, utilizing image prompt adaption. (a) *IPDREAMER pipeline.* We first utilize Stable Diffusion and ControlNet [81] to generate an RGB image I_{rgb} based on the user-provided textual prompt and condition. Then we obtain a 3D object in a coarse-to-fine manner. In Stage 1, we harness Zero-1-to-3 [34] to optimize a NeRF model, yielding the coarse 3D object. (b) *Details of Mesh Training.* In Stage 2, we utilize DMTet [59] to extract the 3D mesh from the NeRF. Then, using the image prompt features from the provided image and its corresponding normal map, we apply IPSD to individually optimize the texture and geometry of the 3D mesh. In addition, we propose an optional strategy LEPTI, to enable desired 3D object synthesis when the complex image prompt is significantly different from the appearance of the coarse NeRF model. Stage 2 enables us to synthesize a desired high-resolution 3D object.

Image Generation. With the current advancements in text-to-image generation and editing techniques, we now have a variety of methods available to create desired images that can be used to guide the 3D generation process. In this study, we utilize Stable Diffusion and ControlNet [81] to generate images based on textual prompts and user-provided conditions. This approach allows users to have better control of the appearance of the 3D object according to the generated image prompt I_{rgb} .

Training of the Coarse NeRF Model. Let x_{rgb} be the rendered image from a randomly sampled viewpoint. We utilize the SDS loss in conjunction with the Zero-1-to-3 model $\epsilon_{zero123}$ to optimize the NeRF parameters θ , with the following gradient:

$$\nabla_{\theta} \mathcal{L}_{Zero123-SDS}(\theta) = \mathbb{E}_{t, \epsilon} [w(t) (\epsilon_{zero123}(z_{rgb,t}; (I_{rgb}, R, T), t) - \epsilon) \frac{\partial z_{rgb}}{\partial \theta}], \quad (2)$$

where $z_{rgb,t}$ denotes the noisy latent code of x_{rgb} in timestep t (we employ the encoder of Stable Diffusion [56] to encode the observed image into the latent code), $R \in \mathbb{R}^{3 \times 3}$ and $T \in \mathbb{R}^3$ respectively denote the relative camera rotation and translation from the default viewpoint (i.e., the viewpoint corresponding to I_{rgb}) to a random viewpoint. Upon completing this training stage, we obtain a coarse yet view-consistent NeRF model.

3.4 Mesh Training with Image Prompt Adaption

In this section, we disentangle the modeling and optimization of the geometry and texture of a 3D object. Formally, we represent the 3D shape using a deformable tetrahedral grid (V, T), where V is the set of vertices and T is the set of tetrahedrons in the grid. Each vertex $v_i \in V$ contains a signed

distance field (SDF) value $s_i \in S$ and a deformation $\Delta v_i \in \Delta V$ of the vertex from its initial canonical coordinate. During optimization, we render the extracted surface mesh into a high-resolution image using the differentiable rasterizer [44]. We optimize ΔV , S and θ via backpropagation using the IPSD gradients (Eq. 3, Eq. 4, Eq. 6, Eq. 7 and Eq. 8).

As shown in the upper-right box in Fig. 2(b), for geometry optimization, we render and encode the surface normal map extracted from DM Tet [59] as the input of ϵ_{ip} , which can generate an object with more detail. For texture optimization, we utilize y_{rgb} and a geometry prompt difference δ_{geo} to optimize the texture of the 3D object. Note that the I_{rgb} in this section can be replaced with another complex image, as discussed in Fig. 4, which demonstrates the excellent guidance capability of IPSD for 3D object synthesis.

Geometry Optimization. Both Fantasia3D [7] and ProlificDreamer [74] optimize the estimated normal map using SDS for geometry optimization. However, optimizing the normal map with a text-to-image DM can be rather challenging because the DM’s pre-training dataset lacks normal map images. To address this, we adopt an additional normal image prompt feature $y_n = \mathcal{E}_{image}(I_n)$ to provide richer and more reliable information for normal map optimization, instead of solely using the textual prompt y [7, 74].

The geometry optimization process computes the gradients of the IPSD geometry loss as:

$$\nabla_{\Delta V} \mathcal{L}_{IPSD-Geo}(\Delta V, S) = \mathbb{E}_{t,\epsilon}[w(t) (\epsilon_{ip}(z_{n,t}; y_n, y, t) - \epsilon) \frac{\partial z_n}{\partial \Delta V}], \quad (3)$$

$$\nabla_S \mathcal{L}_{IPSD-Geo}(\Delta V, S) = \mathbb{E}_{t,\epsilon}[w(t) (\epsilon_{ip}(z_{n,t}; y_n, y, t) - \epsilon) \frac{\partial z_n}{\partial S}], \quad (4)$$

where $z_{n,t}$ denotes the noisy latent code of $x_{n,ran}$ in timestep t . The IPSD (image prompt score distillation) geometry loss is an extension of the SDS loss [50], with $\Delta V, S$ and y_n added. IPSD has a lower computational cost compared to VSD [74], as VSD requires the optimization of additional training parameters (i.e., the parameters of its LoRA model).

Texture Optimization. After optimizing the estimated normal map, the shape of the 3D mesh becomes more reasonable. Then we further optimize the texture through IPSD. We first extract the image prompt features $y_{rgb} = \mathcal{E}_{image}(I_{rgb})$, as a basic guidance for the texture optimization. Then we devise a geometry prompt difference δ_{geo} for y_{rgb} to compensate for the morphological disparity between x_{rgb} and I_{rgb} . Let $x_{n,def}$, and $x_{n,ran}$ be the rendered normal map of the 3D mesh from the default viewpoint and a randomly sampled viewpoint, respectively. We extract their image prompt features, $y_{n,def} = \mathcal{E}_{image}(x_{n,def})$ and $y_{n,ran} = \mathcal{E}_{image}(x_{n,ran})$. The difference between $y_{n,ran}$ and $y_{n,def}$ is called the geometry prompt difference δ_{geo} :

$$\delta_{geo} = y_{n,ran} - y_{n,def}. \quad (5)$$

The texture optimization process computes the gradients of the IPSD texture loss as:

$$\nabla_{\theta} \mathcal{L}_{IPSD-Tex}(\theta, \Delta V, S) = \mathbb{E}_{t,\epsilon}[w(t) (\epsilon_{ip}(z_{rgb,t}; y_{rgb} + \delta_{geo}, y, t) - \epsilon) \frac{\partial z_{rgb}}{\partial \theta}], \quad (6)$$

$$\nabla_{\Delta V} \mathcal{L}_{IPSD-Tex}(\theta, \Delta V, S) = \mathbb{E}_{t,\epsilon}[w(t) (\epsilon_{ip}(z_{rgb,t}; y_{rgb} + \delta_{geo}, y, t) - \epsilon) \frac{\partial z_{rgb}}{\partial \Delta V}], \quad (7)$$

$$\nabla_S \mathcal{L}_{IPSD-Tex}(\theta, \Delta V, S) = \mathbb{E}_{t,\epsilon}[w(t) (\epsilon_{ip}(z_{rgb,t}; y_{rgb} + \delta_{geo}, y, t) - \epsilon) \frac{\partial z_{rgb}}{\partial S}], \quad (8)$$

where $z_{rgb,t}$ denotes the noisy latent code of x_{rgb} (random viewpoint) in timestep t . The geometry prompt difference δ_{geo} can effectively represent the Morphological distance between $x_{n,ran}$ and $x_{n,def}$ in the image prompt feature space. Thus it is used to compensate y_{rgb} (default viewpoint) such that $y_{rgb} + \delta_{geo}$ represents the RGB image x_{rgb} .

Cross Attention for the Image Prompt in 3D Generation. Here we explain how our method can effectively use a complex, high-quality image to guide 3D object synthesis, by introducing cross attention for the image prompt. Given the query features Z which are derived from the latent

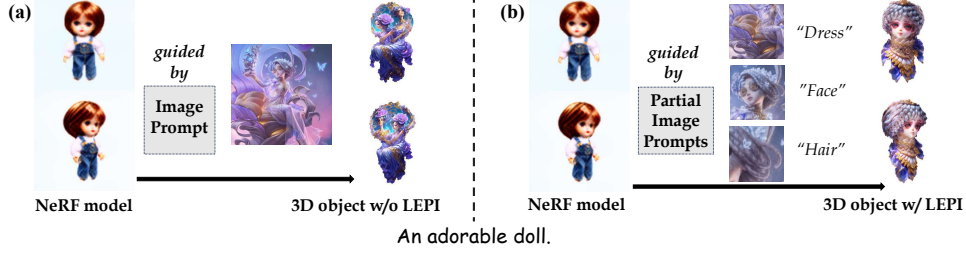


Figure 3: Illustration of the effectiveness of LEPI.

representations of the 2D rendering results of the 3D object from various viewpoints, and the image prompt embedding y_{rgb} , the cross-attention for the image prompt is formulated as follows:

$$Z' = \text{Softmax}\left(\frac{\mathbf{Q}\mathbf{K}^\top}{\sqrt{d}}\right)\mathbf{V}, \quad (9)$$

where $\mathbf{Q} = Z\mathbf{W}_q$, $\mathbf{K} = y_{rgb}\mathbf{W}_k^{ip}$, $\mathbf{V} = y_{rgb}\mathbf{W}_v^{ip}$ represent the queries, keys, and values within the cross-attention module, respectively, Z' denotes the output features of the module, and the \mathbf{W}_q , \mathbf{W}_k^{ip} , and \mathbf{W}_v^{ip} are the projection matrices used for linear transformations. The reasons why IPSD can utilize complex images to guide the generation of 3D objects, while existing single-image-to-3D methods cannot, are two-fold: First, the encoder of the image prompt adaption method effectively extracts the image features y_{rgb} from the reference high-resolution image prompt. Concurrently, as the attention map can accurately align the features y_{rgb} with specific positions of rendered images [16] from the 3D object, the features from the original complex image are precisely positioned on the most relevant parts of the 3D object.

Local Editing with Partial Images. When the rendered 2D images from the NeRF model are quite different from the image prompt, merely utilizing the cross attention for the image prompt cannot well align the features y_{rgb} with specific positions on the 3D object. As shown in Fig. 3(a), it becomes evident that IPDreamer struggles with this challenging sample. To solve this problem, we design a strategy named Local Editing with Partial Images (LEPI). Specifically, we divide I_{rgb} into partial images I_i^{rgb} and employ a large multimodal model (GPT-4v) to provide localization words y_i^{txt} for corresponding I_i^{rgb} . We adopt the cross attention in LDM [56] to obtain localization masks:

$$m_i = \text{BI}\left(\text{Softmax}\left(\frac{\mathbf{Q}\mathbf{K}_{txt,i}^\top}{\sqrt{d}}\right)\right), \quad \mathbf{Q} = Z\mathbf{W}_q, \quad \mathbf{K}_{txt,i} = y_i^{txt}\mathbf{W}_k^{txt}, \quad i = 1, 2, \dots, n_{ip}, \quad (10)$$

where BI denotes a binarization operator and n_{ip} is the number of the partial images. Subsequently, the mask m_i , obtained from the textual description y_i^{txt} , is used to adjust the computation of the cross attention corresponding to the feature y_i^{rgb} of the partial image prompt I_i^{rgb} :

$$Z' = \frac{1}{n_{ip}} \sum_{i=1}^{n_{ip}} m_i \text{Softmax}\left(\frac{\mathbf{Q}\mathbf{K}_{ip,i}^\top}{\sqrt{d}}\right)\mathbf{V}_{ip,i}, \quad (11)$$

where $\mathbf{Q} = Z\mathbf{W}_q$, $\mathbf{K}_{ip,i} = y_i^{rgb}\mathbf{W}_k^{ip}$, $\mathbf{V}_{ip,i} = y_i^{rgb}\mathbf{W}_v^{ip}$. With the help of LEPI, we successfully localize the features of the partial images onto the 3D object, as shown in Fig. 3(b). **We provide more details of LEPI in the supplementary material (Appendix).**

4 Experiments

We conduct experiments of texture editing, comparison with SOTA methods, and ablation study in this section. Note that the optional module LEPI is not used unless explicitly indicated.

4.1 Texture Editing

In Stage 2 of our framework (see Fig. 2), after a NeRF model is obtained in Stage 1, we can use another image prompt with a similar object but a different texture for texture editing. As depicted in



Figure 4: Edited 3D objects with different image prompts. (a) Scribble object outlines and corresponding image prompts for NeRF models generation. (b) Rendering of NeRFs from Stage 1. We show four samples for each textual prompt. In each sample, the top left is a selected image prompt, and the bottom left and the right illustrate the 3D object optimized by IPDREAMER based on the NeRF from Stage 1.



Figure 5: Comparison with SOTA methods. Our results are not only high-quality but also controllable.

Fig. 4, we show reconstructed 3D samples that use new image prompts to guide generation. This demonstrates IPDREAMER’s ability to produce high-quality 3D objects that align with the styles of the provided images. Remarkably, IPDREAMER can appropriately transfer the styles of the image prompts to the synthesized 3D objects, regardless of the structure difference between the image prompts and the pretrained NeRF models. To the best of our knowledge, this style transfer task is not achievable by existing single-image-to-3D methods. In Sample 2 for the textual prompt “An iron breastplate”, although both the textual and image prompt features are provided for 3D object synthesis, the generated result resembles a leather breastplate more closely, which aligns with the image prompt rather than the “iron” mentioned in the textual prompt. This illustrates that the image prompt exerts a stronger influence on the synthesis of the 3D object than the textual prompt.

4.2 Comparison with SOTA Text-to-3D Methods

In Fig. 5, we compare IPDREAMER with four SOTA text-to-3D methods: DreamFusion [50], Magic3D [31], Fantasia3D [7], and ProlificDreamer [74]. With the help of IPSD, IPDREAMER can generate highly controllable and realistic 3D objects that are consistent with the given textual prompts. More samples are provided in Appendix B. We randomly select 20 textual prompts (see Table 3 of Appendix) and

Table 1: Quantitative comparison of text-to-3D generation.

Metrics	DreamFusion	Magic3D	Fantasia3D	ProlificDreamer	IPDreamer (Ours)
FID ↓	313.58	328.00	292.86	284.52	257.17
CLIP-Score ↑	0.2532	0.2722	0.2690	0.2725	0.2859

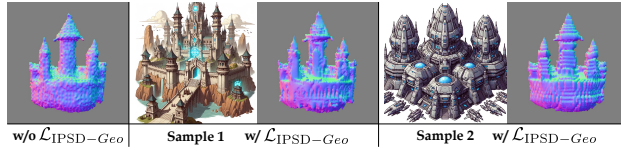


Figure 6: Visualization of the initial normal map of the 3D object at the beginning of geometry optimization, along with the image prompt and the refined normal map after geometry optimization for each sample.

Table 2: Ablation study of δ_{geo} .

Methods	CLIP score ↑
w/o δ_{geo}	0.8228
w/ δ_{geo}	0.8389

conduct a quantitative comparison in Table 1. Our IPDreamer outperforms the SOTA methods. The lower FID score suggests the best quality of the 3D objects generated by IPDreamer, while the higher CLIP score demonstrates that the generation results of IPDreamer are more aligned with the provided textual prompts. How to calculate CLIP score and FID is detailed in Appendix F, and we also provide a user study in Appendix C.

4.3 Ablation Study

We conduct an ablation study to evaluate the impact of $\mathcal{L}_{IPSD-Geo}$ and δ_{geo} on optimizing 3D objects. Their effectiveness is illustrated in Fig. 6 and Table 2. In Fig. 6, we showcase the optimized normal maps of two samples. After geometry optimization, Sample 1 and Sample 2 learn the high-frequency details from their corresponding image prompts. The difference in the optimized normal maps between Sample 1 and Sample 2 is readily discernible in Fig. 6, illustrating the efficacy of $\mathcal{L}_{IPSD-Geo}$ in learning geometry representations from image prompts for style transfer. In Table 2, we compare the CLIP score of 3D objects optimized with and without δ_{geo} . We conduct the quantitative comparison using the samples mentioned in Section 4.2 and employ CLIP score to compare the alignment of rendered images of 3D objects generated with and without δ_{geo} in different viewpoints with the reference image prompt. The experimental results show that with δ_{geo} , the rendered images of the 3D object in different viewpoints are more consistent with the reference image prompt.

Besides, to demonstrate the effectiveness of LEPI, we showcase two samples where the provided image prompts vastly differ from the coarse NeRF models in Fig. 7. It is obvious that with LEPI, IPDreamer generates high-quality 3D objects that retain the semantic essence of the original coarse NeRF models and achieve the intended outcomes. More samples based on LEPI are shown in Appendix A.



Figure 7: Ablation study of LEPI.

5 Conclusion

In this work, we propose IPDreamer to achieve controllable high-quality 3D object generation. We introduce Image Prompt Score Distillation (IPSD) that employs image prompt adaption to provide detailed appearance information for better 3D object optimization. IPSD utilizes the reference image prompts and their corresponding normal maps to optimize the texture and geometry of 3D meshes, respectively. The experiments show that our IPDreamer is capable of generating appearance-controllable high-quality 3D objects. Improvements in 3D generation have often been constrained by the difficulty of obtaining 3D data, whereas optimizing the generation of rough 3D models and generating specific images are much simpler tasks. The significant breakthrough of this work lies in decomposing the 3D generation task into acquiring rough 3D models and optimizing 3D objects with the introduction of image prompt adaptation. Our IPDreamer not only improves the quality of generated 3D objects but also sets a new direction for future enhancements in 3D generation.

References

- [1] Avrahami, O., Lischinski, D., Fried, O.: Blended diffusion for text-driven editing of natural images. In: CVPR (2022)
- [2] Brooks, T., Holynski, A., Efros, A.A.: Instructpix2pix: Learning to follow image editing instructions. In: CVPR (2023)
- [3] Brown, T., Mann, B., Ryder, N., Subbiah, M., Kaplan, J.D., et al.: Language models are few-shot learners. In: NeurIPS (2020)
- [4] Chan, E.R., Lin, C.Z., Chan, M.A., Nagano, K., Pan, B., et al.: Efficient geometry-aware 3d generative adversarial networks. In: CVPR (2022)
- [5] Chan, E.R., Monteiro, M., Kellnhofer, P., Wu, J., Wetzstein, G.: pi-gan: Periodic implicit generative adversarial networks for 3d-aware image synthesis. In: CVPR (2021)
- [6] Chen, D.Z., Siddiqui, Y., Lee, H.Y., Tulyakov, S., Nießner, M.: Text2tex: Text-driven texture synthesis via diffusion models. arXiv preprint arXiv:2303.11396 (2023)
- [7] Chen, R., Chen, Y., Jiao, N., Jia, K.: Fantasia3d: Disentangling geometry and appearance for high-quality text-to-3d content creation. arXiv preprint arXiv:2303.13873 (2023)
- [8] Chen, Y., Zhang, C., Yang, X., Cai, Z., Yu, G., Yang, L., Lin, G.: It3d: Improved text-to-3d generation with explicit view synthesis. arXiv preprint arXiv:2308.11473 (2023)
- [9] Dhariwal, P., Nichol, A.: Diffusion models beat gans on image synthesis. In: NeurIPS (2021)
- [10] Gal, R., Patashnik, O., Maron, H., Bermano, A.H., Chechik, G., Cohen-Or, D.: Stylegan-nada: Clip-guided domain adaptation of image generators. ToG (2022)
- [11] Gao, S., Liu, X., Zeng, B., Xu, S., Li, Y., Luo, X., Liu, J., Zhen, X., Zhang, B.: Implicit diffusion models for continuous super-resolution. arXiv preprint arXiv:2303.16491 (2023)
- [12] Geyer, M., Bar-Tal, O., Bagon, S., Dekel, T.: Tokenflow: Consistent diffusion features for consistent video editing. In: ICLR (2023)
- [13] Gu, J., Liu, L., Wang, P., Theobalt, C.: Stylenerf: A style-based 3d-aware generator for high-resolution image synthesis. arXiv preprint arXiv:2110.08985 (2021)
- [14] Hao, Z., Mallya, A., Belongie, S., Liu, M.Y.: Gancraft: Unsupervised 3d neural rendering of minecraft worlds. In: CVPR (2021)
- [15] Haque, A., Tancik, M., Efros, A.A., Holynski, A., Kanazawa, A.: Instruct-nerf2nerf: Editing 3d scenes with instructions. arXiv preprint arXiv:2303.12789 (2023)
- [16] Hertz, A., Mokady, R., Tenenbaum, J., Aberman, K., Pritch, Y., Cohen-Or, D.: Prompt-to-prompt image editing with cross attention control. arXiv preprint arXiv:2208.01626 (2022)

- [17] Heusel, M., Ramsauer, H., Unterthiner, T., Nessler, B., Hochreiter, S.: Gans trained by a two time-scale update rule converge to a local nash equilibrium (2017)
- [18] Ho, J., Chan, W., Saharia, C., Whang, J., Gao, R., et al.: Imagen video: High definition video generation with diffusion models. arXiv:2210.02303 (2022)
- [19] Ho, J., Jain, A., Abbeel, P.: Denoising diffusion probabilistic models. In: NeurIPS (2020)
- [20] Ho, J., Salimans, T., Gritsenko, A., Chan, W., Norouzi, M., Fleet, D.J.: Video diffusion models. In: NeurIPS (2022)
- [21] Hu, E.J., Shen, Y., Wallis, P., Allen-Zhu, Z., Li, Y., Wang, S., Wang, L., Chen, W.: Lora: Low-rank adaptation of large language models. arXiv preprint arXiv:2106.09685 (2021)
- [22] Huang, L., Chen, D., Liu, Y., Shen, Y., Zhao, D., Zhou, J.: Composer: Creative and controllable image synthesis with composable conditions. arXiv preprint arXiv:2302.09778 (2023)
- [23] Jain, A., Mildenhall, B., Barron, J.T., Abbeel, P., Poole, B.: Zero-shot text-guided object generation with dream fields. In: CVPR (2022)
- [24] Kerbl, B., Kopanas, G., Leimkühler, T., Drettakis, G.: 3d gaussian splatting for real-time radiance field rendering. ToG (2023)
- [25] Kirillov, A., Mintun, E., Ravi, N., Mao, H., Rolland, C., Gustafson, L., Xiao, T., Whitehead, S., Berg, A.C., Lo, W.Y., et al.: Segment anything. arXiv preprint arXiv:2304.02643 (2023)
- [26] Kong, Z., Ping, W., Huang, J., Zhao, K., Catanzaro, B.: Diffwave: A versatile diffusion model for audio synthesis. arXiv:2009.09761 (2020)
- [27] Kulikov, V., Yadin, S., Kleiner, M., Michaeli, T.: Sinddm: A single image denoising diffusion model. In: PMLR (2022)
- [28] Li, H., Yang, Y., Chang, M., Chen, S., Feng, H., Xu, Z., Li, Q., Chen, Y.: Srdiff: Single image super-resolution with diffusion probabilistic models. Neurocomputing (2022)
- [29] Li, M., Duan, Y., Zhou, J., Lu, J.: Diffusion-sdf: Text-to-shape via voxelized diffusion. arXiv:2212.03293 (2022)
- [30] Liang, Y., Yang, X., Lin, J., Li, H., Xu, X., Chen, Y.: Luciddreamer: Towards high-fidelity text-to-3d generation via interval score matching. arXiv preprint arXiv:2311.11284 (2023)
- [31] Lin, C.H., Gao, J., Tang, L., Takikawa, T., Zeng, X., Huang, X., Kreis, K., Fidler, S., Liu, M.Y., Lin, T.Y.: Magic3d: High-resolution text-to-3d content creation. In: CVPR (2023)
- [32] Liu, J., Li, C., Ren, Y., Chen, F., Liu, P., Zhao, Z.: Diffsinger: Diffusion acoustic model for singing voice synthesis. arXiv:2105.02446 (2021)
- [33] Liu, M., Xu, C., Jin, H., Chen, L., Xu, Z., Su, H.: One-2-3-45: Any single image to 3d mesh in 45 seconds without per-shape optimization. arXiv preprint arXiv:2306.16928 (2023)
- [34] Liu, R., Wu, R., Van Hoorick, B., Tokmakov, P., Zakharov, S., Vondrick, C.: Zero-1-to-3: Zero-shot one image to 3d object. arXiv preprint arXiv:2303.11328 (2023)
- [35] Liu, Y., Lin, C., Zeng, Z., Long, X., Liu, L., Komura, T., Wang, W.: Syncdreamer: Generating multiview-consistent images from a single-view image. arXiv preprint arXiv:2309.03453 (2023)
- [36] Lugmayr, A., Danelljan, M., Romero, A., Yu, F., Timofte, R., Van Gool, L.: Repaint: Inpainting using denoising diffusion probabilistic models. In: CVPR (2022)
- [37] Luo, S., Hu, W.: Diffusion probabilistic models for 3d point cloud generation. In: CVPR (2021)
- [38] Melas-Kyriazi, L., Laina, I., Rupprecht, C., Vedaldi, A.: Realfusion: 360deg reconstruction of any object from a single image. In: CVPR (2023)
- [39] Mildenhall, B., Srinivasan, P.P., Tancik, M., Barron, J.T., Ramamoorthi, R., Ng, R.: Nerf: Representing scenes as neural radiance fields for view synthesis. COMMUN ACM (2021)

- [40] Mohammad Khalid, N., Xie, T., Belilovsky, E., Popa, T.: Clip-mesh: Generating textured meshes from text using pretrained image-text models. In: SIGGRAPH Asia (2022)
- [41] Mokady, R., Hertz, A., Aberman, K., Pritch, Y., Cohen-Or, D.: Null-text inversion for editing real images using guided diffusion models. In: CVPR (2023)
- [42] Mou, C., Wang, X., Xie, L., Zhang, J., Qi, Z., Shan, Y., Qie, X.: T2i-adapter: Learning adapters to dig out more controllable ability for text-to-image diffusion models. arXiv preprint arXiv:2302.08453 (2023)
- [43] Müller, T., Evans, A., Schied, C., Keller, A.: Instant neural graphics primitives with a multiresolution hash encoding. ToG (2022)
- [44] Munkberg, J., Hasselgren, J., Shen, T., Gao, J., Chen, W., Evans, A., Müller, T., Fidler, S.: Extracting triangular 3d models, materials, and lighting from images. In: CVPR (2022)
- [45] Nguyen-Phuoc, T., Li, C., Theis, L., Richardt, C., Yang, Y.L.: Hologan: Unsupervised learning of 3d representations from natural images. In: ICCV (2019)
- [46] Nichol, A., Dhariwal, P., Ramesh, A., Shyam, P., Mishkin, P., McGrew, B., Sutskever, I., Chen, M.: Glide: Towards photorealistic image generation and editing with text-guided diffusion models. arXiv preprint arXiv:2112.10741 (2021)
- [47] Niemeyer, M., Geiger, A.: Giraffe: Representing scenes as compositional generative neural feature fields. In: CVPR (2021)
- [48] Peebles, W., Xie, S.: Scalable diffusion models with transformers. arXiv:2212.09748 (2022)
- [49] Podell, D., English, Z., Lacey, K., Blattmann, A., Dockhorn, T., Müller, J., Penna, J., Rombach, R.: Sdxl: Improving latent diffusion models for high-resolution image synthesis. In: ICLR (2024)
- [50] Poole, B., Jain, A., Barron, J.T., Mildenhall, B.: Dreamfusion: Text-to-3d using 2d diffusion. arXiv preprint arXiv:2209.14988 (2022)
- [51] Qi, Z., Zhang, X., Cheng, N., Xiao, J., Wang, J.: Diftalker: Co-driven audio-image diffusion for talking faces via intermediate landmarks. arXiv preprint arXiv:2309.07509 (2023)
- [52] Qian, G., Mai, J., Hamdi, A., Ren, J., Siarohin, A., Li, B., Lee, H.Y., Skorokhodov, I., Wonka, P., Tulyakov, S., Bernard, G.: Magic123: One image to high-quality 3d object generation using both 2d and 3d diffusion priors. arXiv preprint arXiv:2306.17843 (2023)
- [53] Radford, A., Kim, J.W., Hallacy, C., Ramesh, A., Goh, G., et al.: Learning transferable visual models from natural language supervision. In: ICML (2021)
- [54] Ramesh, A., Dhariwal, P., Nichol, A., Chu, C., Chen, M.: Hierarchical text-conditional image generation with clip latents. arXiv preprint arXiv:2204.06125 (2022)
- [55] Ranftl, R., Bochkovskiy, A., Koltun, V.: Vision transformers for dense prediction. In: ICCV (2021)
- [56] Rombach, R., Blattmann, A., Lorenz, D., Esser, P., Ommer, B.: High-resolution image synthesis with latent diffusion models. In: CVPR (2022)
- [57] Saharia, C., Chan, W., Saxena, S., Li, L., Whang, J., Jonathan, H., et al.: Photorealistic text-to-image diffusion models with deep language understanding. In: NeurIPS (2022)
- [58] Saharia, C., Ho, J., Chan, W., Salimans, T., Fleet, D.J., Norouzi, M.: Image super-resolution via iterative refinement. TPAMI (2022)
- [59] Shen, T., Gao, J., Yin, K., Liu, M.Y., Fidler, S.: Deep marching tetrahedra: a hybrid representation for high-resolution 3d shape synthesis. In: NeurIPS (2021)
- [60] Shi, Y., Wang, P., Ye, J., Long, M., Li, K., Yang, X.: Mvdream: Multi-view diffusion for 3d generation. arXiv preprint arXiv:2308.16512 (2023)

- [61] Sohl-Dickstein, J., Weiss, E., Maheswaranathan, N., Ganguli, S.: Deep unsupervised learning using nonequilibrium thermodynamics. In: ICML (2015)
- [62] Song, J., Meng, C., Ermon, S.: Denoising diffusion implicit models. arXiv:2010.02502 (2020)
- [63] Takagi, Y., Nishimoto, S.: High-resolution image reconstruction with latent diffusion models from human brain activity. biorxiv. In: CVPR (2022)
- [64] Takagi, Y., Nishimoto, S.: High-resolution image reconstruction with latent diffusion models from human brain activity. In: CVPR (2023)
- [65] Tang, J., Ren, J., Zhou, H., Liu, Z., Zeng, G.: Dreamgaussian: Generative gaussian splatting for efficient 3d content creation. arXiv preprint arXiv:2309.16653 (2023)
- [66] Tang, J., Wang, T., Zhang, B., Zhang, T., Yi, R., Ma, L., Chen, D.: Make-it-3d: High-fidelity 3d creation from a single image with diffusion prior. arXiv preprint arXiv:2303.14184 (2023)
- [67] Tevet, G., Raab, S., Gordon, B., Shafir, Y., Cohen-Or, D., Bermano, A.H.: Human motion diffusion model. arXiv:2209.14916 (2022)
- [68] Touvron, H., Lavril, T., Izacard, G., Martinet, X., Lachaux, M.A., et al.: Llama: Open and efficient foundation language models. arXiv preprint arXiv:2302.13971 (2023)
- [69] Touvron, H., Martin, L., Stone, K., Albert, P., Almahairi, A., et al.: Llama 2: Open foundation and fine-tuned chat models. arXiv preprint arXiv:2307.09288 (2023)
- [70] Tumanyan, N., Geyer, M., Bagon, S., Dekel, T.: Plug-and-play diffusion features for text-driven image-to-image translation. In: CVPR (2023)
- [71] Vahdat, A., Kreis, K., Kautz, J.: Score-based generative modeling in latent space. In: NeurIPS (2021)
- [72] Wang, Q., Bai, X., Wang, H., Qin, Z., Chen, A.: Instantid: Zero-shot identity-preserving generation in seconds. arXiv preprint arXiv:2401.07519 (2024)
- [73] Wang, W., Bao, J., Zhou, W., Chen, D., Chen, D., Yuan, L., Li, H.: Sindiffusion: Learning a diffusion model from a single natural image. arXiv:2211.12445 (2022)
- [74] Wang, Z., Lu, C., Wang, Y., Bao, F., Li, C., Su, H., Zhu, J.: Prolificdreamer: High-fidelity and diverse text-to-3d generation with variational score distillation. arXiv preprint arXiv:2305.16213 (2023)
- [75] Wu, J.Z., Ge, Y., Wang, X., Lei, S.W., Gu, Y., Shi, Y., Hsu, W., Shan, Y., Qie, X., Shou, M.Z.: Tune-a-video: One-shot tuning of image diffusion models for text-to-video generation. In: ICCV (2023)
- [76] Xie, X., Zhou, P., Li, H., Lin, Z., Yan, S.: Adan: Adaptive nesterov momentum algorithm for faster optimizing deep models. arXiv preprint arXiv:2208.06677 (2022)
- [77] Yang, J., Cheng, Z., Duan, Y., Ji, P., Li, H.: Consistnet: Enforcing 3d consistency for multi-view images diffusion. arXiv preprint arXiv:2310.10343 (2023)
- [78] Yang, L., Yu, Z., Meng, C., Xu, M., Ermon, S., Cui, B.: Mastering text-to-image diffusion: Recaptioning, planning, and generating with multimodal llms. ICML (2024)
- [79] Ye, H., Zhang, J., Liu, S., Han, X., Yang, W.: Ip-adapter: Text compatible image prompt adapter for text-to-image diffusion models. arXiv preprint arXiv:2308.06721 (2023)
- [80] Zhang, K., Mo, L., Chen, W., Sun, H., Su, Y.: Magicbrush: A manually annotated dataset for instruction-guided image editing. arXiv preprint arXiv:2306.10012 (2023)
- [81] Zhang, L., Agrawala, M.: Adding conditional control to text-to-image diffusion models. arXiv preprint arXiv:2302.05543 (2023)

- [82] Zhang, Y., Liu, J., Song, Y., Wang, R., Tang, H., Yu, J., Li, H., Tang, X., Hu, Y., Pan, H., et al.: Ssr-encoder: Encoding selective subject representation for subject-driven generation. arXiv preprint arXiv:2312.16272 (2023)
- [83] Zhao, M., Zhao, C., Liang, X., Li, L., Zhao, Z., Hu, Z., Fan, C., Yu, X.: Efficientdreamer: High-fidelity and robust 3d creation via orthogonal-view diffusion prior. arXiv preprint arXiv:2308.13223 (2023)
- [84] Zhao, S., Chen, D., Chen, Y.C., Bao, J., Hao, S., Yuan, L., Wong, K.Y.K.: Uni-controlnet: All-in-one control to text-to-image diffusion models. arXiv preprint arXiv:2305.16322 (2023)

Appendix (Supplementary Material)

In Appendix A, we show more texture editing examples. Appendix B compares IPDreameer with four SOTA methods for the text-to-3D task. Appendix C provides a user study on text-to-3D generation between IPDreameer and four SOTA methods. Additionally, it evaluates the effectiveness of LEPI in texture editing. In Appendix D, we integrate our IPSD with existing single-image-to-3D methods to enhance their performance. We further compare IPDreameer with Zero-1-to-3 in Appendix E. The implementation details are given in Appendix F. Finally, the limitation and social impact of our work are described in Appendixes G and H, respectively.

Note that in all the experiments, the optional module LEPI is not used unless explicitly indicated.

A More Examples of Texture Editing

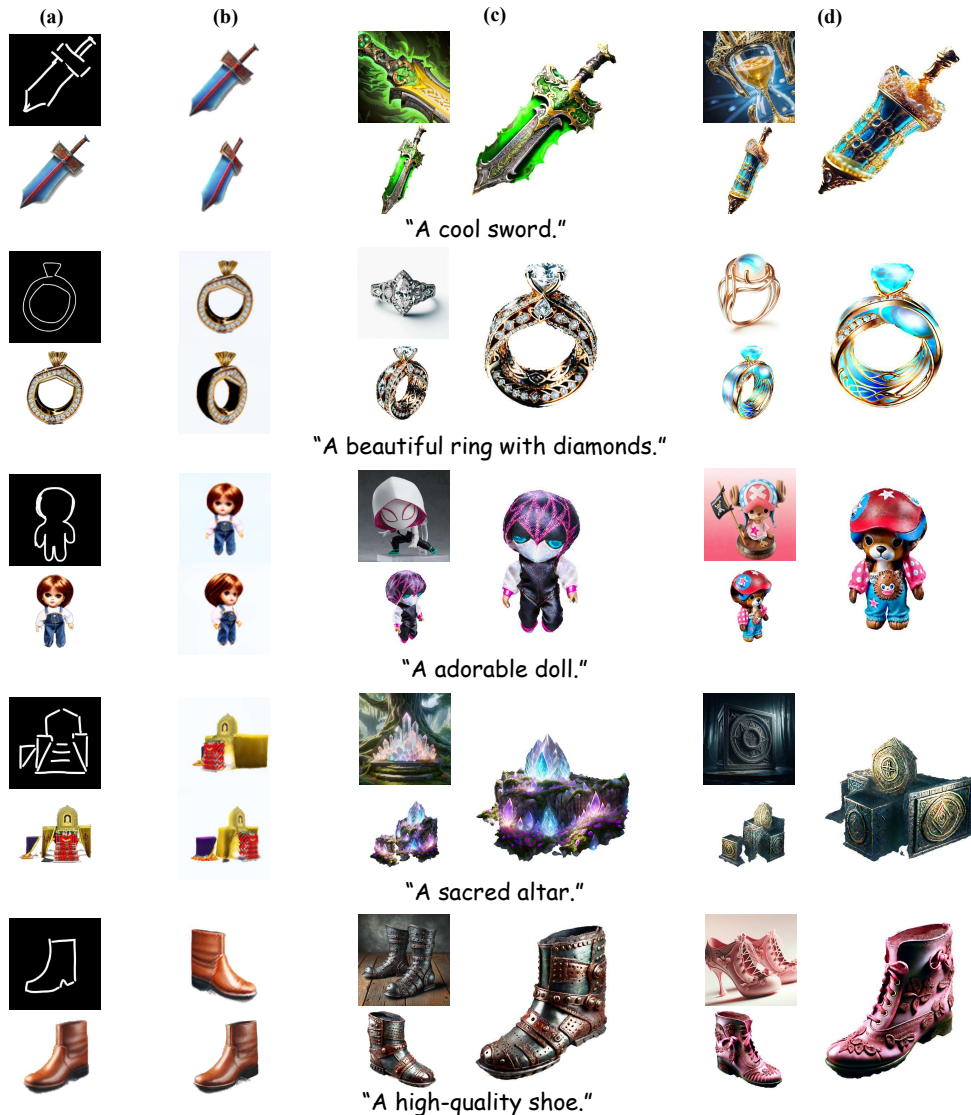


Figure 8: Edited 3D objects with different image prompts. (a) Scribble object outlines and corresponding image prompts generated by ControlNet. (b) Rendering of NeRFs from Stage 1. (c) (d) Two samples demonstrated for each textual prompt. In each sample, the top left is a selected image prompt, and the bottom left and the right illustrate the 3D object optimized by IPDreameer based on the NeRF model from Stage 1.



Figure 9: More samples of 3D object editing. (a) Coarse NeRF models. (b) Provided image prompts. (c) 3D objects generated by IPDreamer.



Figure 10: Comparison of texture editing with and without LEPI.

More Texture Editing Results To further demonstrate IPDreamer’s remarkable ability to manipulate appearance, we conduct more texture editing experiments. These experiments use diverse textual prompts, each accompanied by two distinct image prompts. As evident in Fig. 8, IPDreamer consistently produces impressive 3D object synthesis, regardless of the geometric shape of the NeRF acquired in Stage 1 or the image prompts used for texture editing. The generated results highlight IPDreamer’s powerful texture editing capabilities for 3D objects, suggesting its potential to serve effectively in the 3D gaming and video industries.

Besides, to demonstrate the appearance guidance capability of IPSD in generating 3D objects, we use two samples whose reference image prompts are particularly complex and somewhat different from the initial coarse NeRF models, as shown in Fig. 9. Even in such difficult cases, IPDreamer can still

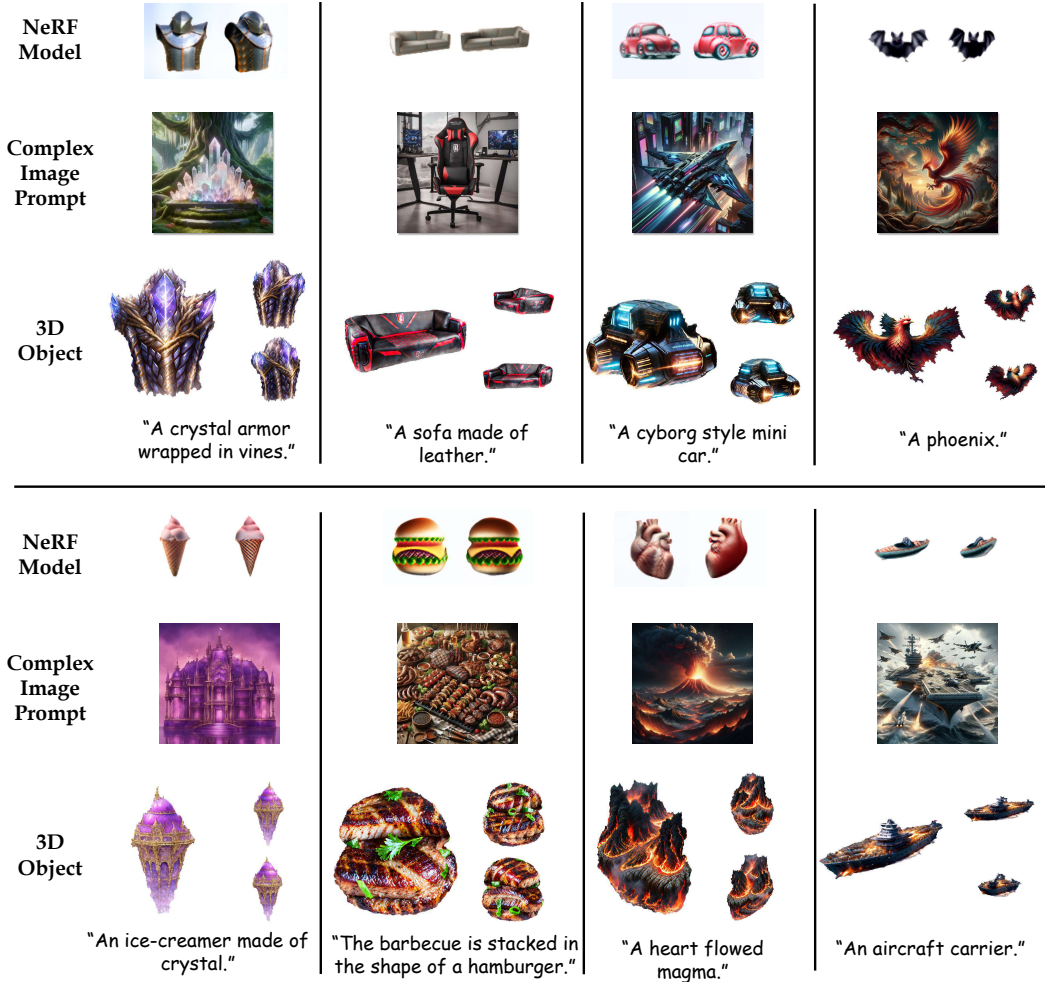


Figure 11: Texture editing with LEPI.

achieve high-quality 3D objects, such as the cyborg-style mini car generated in the first example, and the futuristic toy pistol in the second example. By utilizing IPDREAMER’s style editing ability for 3D objects, the generated results can be more diverse.

More Editing Results with LEPI While IPDREAMER can achieve remarkable texture editing in many difficult cases without LEPI, challenges arise when the appearance of the provided image prompt significantly deviates from the initial coarse NeRF model. To highlight the powerful texture editing capability of LEPI in IPDREAMER, we provide a comparison of generated 3D objects with and without LEPI in Fig. 10. The results confirm the exceptional texture editing capability of LEPI. To further illustrate the superiority of LEPI, we present additional generation results in Fig. 11

B Comparison of Text-to-3D Methods

The textual prompts we use in Section 4.2 of the main paper are shown in Table 3. And we provide more comparison results between IPDREAMER and four SOTA methods [50, 31, 7, 74] in Fig. 12.

C User Study

To further verify the quality of our generated results, we follow previous works [31, 7, 74] and conduct a user study by comparing IPDREAMER with the four SOTA methods [50, 31, 7, 74], under

A praying mantis wearing roller.
 Michelangelo-style statue of a dog reading news on a cellphone.
 A matte painting of a castle made of cheesecake surrounded by a moat made of ice cream.
 A chimpanzee dressed like Henry VIII king of England.
 A 3D model of an adorable cottage with a thatched roof.
 A plate piled high with chocolate chip cookies.
 A vintage record player.
 A car made out of cheese.
 A beautifully carved wooden knight chess piece.
 A car made out of sushi.
 A squirrel-octopus hybrid.
 A small saguaro cactus is planted in a clay pot.
 A DSLR photo of an imperial state crown of England.
 A rotary telephone carved out of wood.
 A raccoon astronaut holding his helmet.
 A classic Packard car.
 A cauldron full of gold coins.
 A blue tulip.
 A stuffed grey rabbit holding a pretend carrot.
 A plush dragon toy.

Table 3: Textual prompts used in the user study.

Table 4: Percentage of the preference in the user study of text-to-3D generation.

Method	Prefer baseline	Prefer ours
DreamFusion	6.45	93.55
Magic3D	10.89	89.11
Fantasia3D	25.82	72.18
ProlificDreamer	41.65	58.35

Table 5: Quantitive comparison of text-to-3D generation.

Method	CLIP-Score \uparrow	UPR (%)
w/o LEPI	0.2041	24.363
w/ LEPI	0.2189	75.637

16 prompts randomly selected from Table 3. Each of 80 volunteers is provided with 16 pairs of results corresponding to the 16 prompts. In each pair, one from IPDreamer and one from a randomly selected baseline. Thus, there are a total of 1280 pairwise comparisons. The volunteers are then asked to choose the better result in terms of faithfulness, quality, and fidelity. It is worth noting that the image prompts used in this study are generated based on the textual prompts, without any other guidance such as scribble images. The percentage of the preference in the user study is shown in Table 4, which indicates that our IPDreamer outperforms all these text-to-3D methods.

Additionally, to validate the effectiveness of LEPI in texture editing, we use the image prompts in Figs. 3, 7, 10, and 11 to perform texture editing and conduct quantitative comparison between with and without LEPI. Table 5 lists the results, showcasing the majority of the volunteers favor the results generated with LEPI (see the user preference rate (UPR) in Table 5). This further substantiates LEPI’s ability to produce high-quality 3D objects, and a higher CLIP score confirms its effectiveness in preserving the semantic integrity of the edited coarse NeRF models.

D Single Image to 3D

IPSD proposed in this paper can be integrated with other existing single-image-to-3D methods to enhance the quality of their generated results. Specifically, the quality of the 3D objects generated by these methods is relatively low in some viewpoints. However, the incorporation of IPSD can improve the quality of the rendered results in any viewpoint. In this work, we combine IPSD with Zero-1-to-3 to achieve single-image-to-3D generation.



Figure 12: Eight text-to-3D examples.

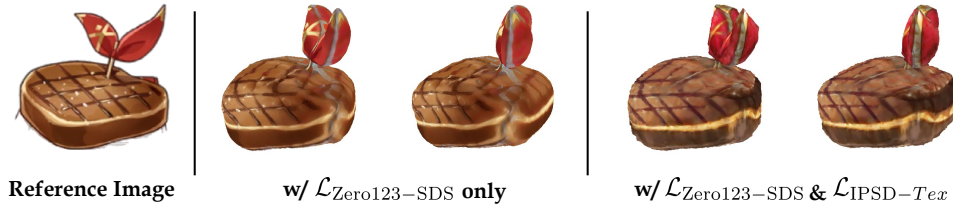


Figure 13: Comparison of single-image-to-3D. The result with both $\mathcal{L}_{\text{Zero123-SDS}}$ and $\mathcal{L}_{\text{IPSD-TeX}}$ reduces unnatural artifacts, leading to a more accurate and realistic 3D model.

Next we describe how we combine $\mathcal{L}_{\text{IPSD-TeX}}$ and $\mathcal{L}_{\text{Zero123-SDS}}$ in texture optimization. Using $\mathcal{L}_{\text{Zero123-SDS}}$ alone to supervise the single-image-to-3D generation may lead to the results that the generated 3D objects are inconsistent when viewed from different directions, as demonstrated in Fig. 13. Therefore, we leverage both $\mathcal{L}_{\text{IPSD-TeX}}$ and $\mathcal{L}_{\text{Zero123-SDS}}$ to supervise the 3D generation simultaneously. The supervision gradients of the combined loss $\mathcal{L}_{\text{IPSD-TeX-Zero123}}$ are defined as follows:

$$\begin{aligned} \nabla_{\theta} \mathcal{L}_{\text{IPSD-TeX-Zero123}}(\theta, \Delta V, S) = & \mathbb{E}_{t_1, t_2, \epsilon_1, \epsilon_2} [(\alpha_1(w(t_1)) \epsilon_{ip}(z_{rgb, t_1}; y_{rgb} + \delta_{geo}, y, t_1) - \epsilon_1) \\ & + \alpha_2(w(t_2)) \epsilon_{zero123}(z_{rgb, t_2}; I_{rgb}, R, T, t_2) - \epsilon_2) \frac{\partial z_{rgb}}{\partial \theta}], \end{aligned} \quad (12)$$

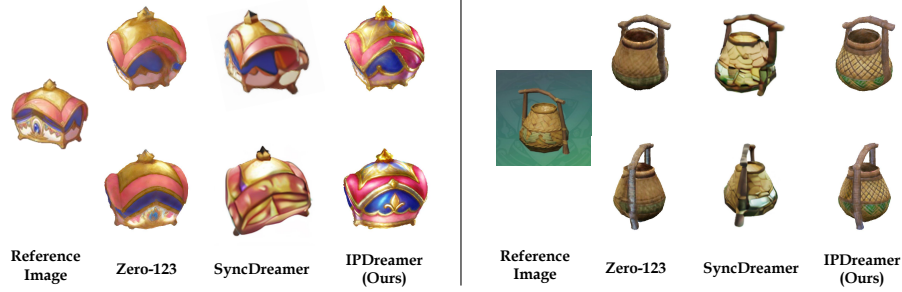


Figure 14: 3D object optimization with different guidance methods based on the same image (left). The result guided by IPSD achieves the best quality.

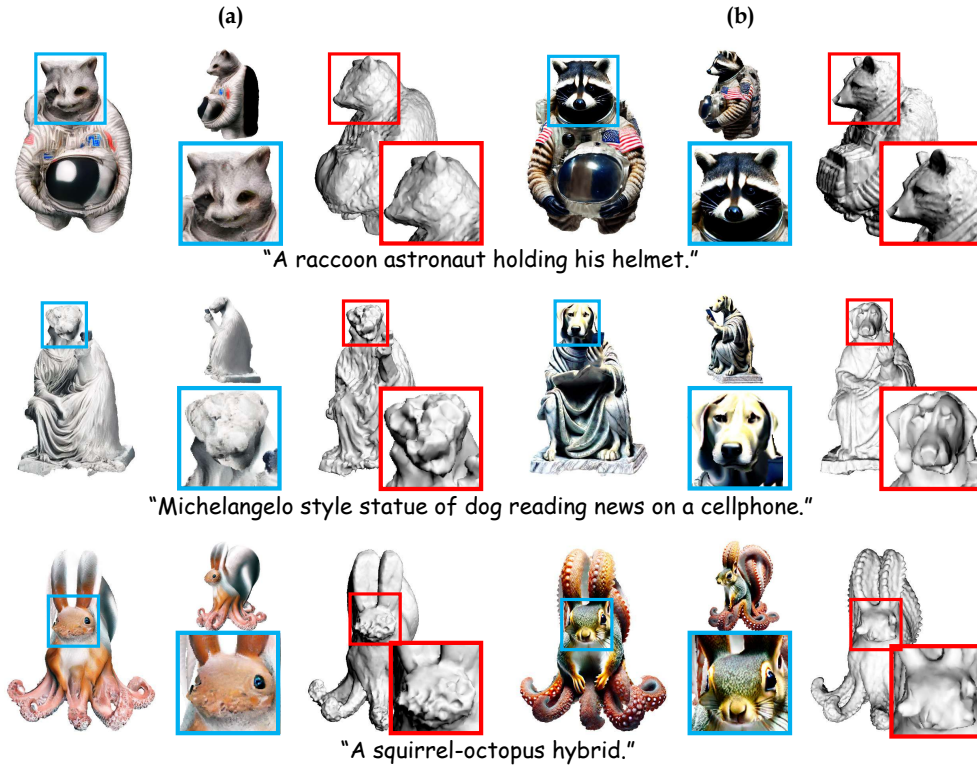


Figure 15: Comparison with Zero-1-to-3 in text-to-3D generation. (a) 3D objects generated by Zero-1-to-3. (b) 3D objects generated by IPDreamer.

$$\begin{aligned} \nabla_{\Delta V} \mathcal{L}_{\text{IPSD-}Tex\text{-}Zero123}(\theta, \Delta V, S) = & \\ & \mathbb{E}_{t_1, t_2, \epsilon_1, \epsilon_2} [(\alpha_1(w(t_1) \epsilon_{ip}(z_{rgb, t_1}; y_{rgb} + \delta_{geo}, y, t_1) - \epsilon_1) \\ & + \alpha_2(w(t_2) \epsilon_{zero123}(z_{rgb, t_2}; I_{rgb}, R, T, t_2) - \epsilon_2)) \frac{\partial z_{rgb}}{\partial \Delta V}], \end{aligned} \quad (13)$$

$$\begin{aligned} \nabla_S \mathcal{L}_{\text{IPSD-}Tex\text{-}Zero123}(\theta, \Delta V, S) = & \\ & \mathbb{E}_{t_1, t_2, \epsilon_1, \epsilon_2} [(\alpha_1(w(t_1) \epsilon_{ip}(z_{rgb, t_1}; y_{rgb} + \delta_{geo}, y, t_1) - \epsilon_1) \\ & + \alpha_2(w(t_2) \epsilon_{zero123}(z_{rgb, t_2}; I_{rgb}, R, T, t_2) - \epsilon_2)) \frac{\partial z_{rgb}}{\partial S}], \end{aligned} \quad (14)$$

where θ , δ_{geo} , ΔV , S , R , and T are the corresponding parameters mentioned in the main paper, and α_1 and α_2 are the balancing parameters. Eq. 12, Eq. 13, and Eq. 14 are modified based on Eq. 8, Eq. 9, and Eq. 10 in the main paper, respectively.

As visualized in Fig. 14, compared with the 3D objects optimized by Zero-1-to-3 [34] and Sync-Dreamer [35], our IPDreamer can add more contextually appropriate details to the 3D object while preserving the identity of the reference image to achieve high-quality 3D object synthesis.

E Comparison with Zero-1-to-3 in Text-to-3D Generation

Existing single-image-to-3D generation methods are also capable of achieving text-to-3D generation. To demonstrate the effectiveness of IPSD, we present a comparison between IPDreamer and Zero-1-to-3 in Fig. 15. We zoom in the selected parts of the 3D objects and meshes to better compare the texture and geometry quality of the 3D objects produced by Zero-1-to-3 and our IPDreamer. Zero-1-to-3’s objects are quite blurry in many rendered images, and its meshes are very rough, indicating that current single-image-to-3D methods struggle with handling complex images. In contrast, the 3D objects generated by IPDreamer are of noticeably higher quality and more reasonable, with better geometric structures, thus proving the effectiveness of IPSD.

F Implementaion Details

F.1 Optimization

In this work, we conduct all of our experiments on one A100-SXM4-40GB GPU. In Stage 1, we optimize $5k$ steps with Adam optimizer [76] to obtain a NeRF model. In Stage 2, we optimize $10k$ steps for geometry optimization and $15k$ steps for texture optimization. During each optimization progress in Stage 2, we initially sample the timesteps $t \sim \mathcal{U}(0.02, 0.98)$ for the first $5k$ steps, and then sample t from $t \sim \mathcal{U}(0.02, 0.5)$ for the rest steps. Each optimization process in Stage 2 requires approximately 9GB GPU memory with batch size 1 and a rendering resolution of 512.

F.2 Metrics

We perform quantitative comparisons to evaluate IPDreamer’s performance, with the following metrics:

- CLIP score [10]: We employ CLIP score in Section 4.2 of the main paper. By assessing the alignment between the textual descriptions and the rendered images of 3D objects from various viewpoints, we can judge whether text-to-3D methods successfully generate 3D objects that match the input textual prompts.
- Fréchet Inception Distance (FID) [17]: To evaluate the quality of the generated results, we utilize FID to compare the similarity between the rendering images of 3D objects and the images generated by the text-to-image model, Stable Diffusion.

F.3 Details of LEPI

In this section, we briefly describe how Local Editing with Partial Images (LEPI) is implemented. Firstly, we utilize GPT-4v to analyze I_{rgb} and the rendered images of the coarse NeRF model. Based on the analysis results, we employ SAM [25] to divide I_{rgb} into n_{ip} parts, yielding partial images $I_1^{rgb}, \dots, I_{n_{ip}}^{rgb}$, along with the corresponding partial textual prompts $y_1^{txt}, \dots, y_{n_{ip}}^{txt}$. Besides, $y_1^{txt}, \dots, y_{n_{ip}}^{txt}$ and $I_1^{rgb}, \dots, I_{n_{ip}}^{rgb}$ can also be adjusted by users.

Since differences may exist in the semantic information between I_{rgb} and the coarse NeRF model (e.g., “magnificent magic castle” vs “adorable cottage”) and the quality of the partial images $I_1^{rgb}, \dots, I_{n_{ip}}^{rgb}$ may be low (e.g., low resolution), it is necessary to enhance them before starting texture optimization. We adopt ControlNet [81]⁵ in conjunction with $I_1^{rgb}, \dots, I_{n_{ip}}^{rgb}$ and $y_1^{txt}, \dots, y_{n_{ip}}^{txt}$ to generate new $I_1^{rgb}, \dots, I_{n_{ip}}^{rgb}$. By this preprocessing, the quality of the final 3D object can be improved.

Subsequently, we extract image prompt features $y_1^{rgb}, \dots, y_{n_{ip}}^{rgb}$ from corresponding partial image prompts $I_1^{ip}, \dots, I_{n_{ip}}^{ip}$. Then, we localize the features onto the 3D object according to $y_1^{txt}, \dots, y_{n_{ip}}^{txt}$,

⁵https://huggingface.co/l1lyasviel/control_v11f1e_sd15_tile



Figure 16: Visualization of localization masks.

based on Equation 10 and Equation 11. Fig. 16 shows an example of the effect of localization masks calculated in LEPI. The IPSD supervision in this part can be written as:

$$\nabla_{\theta} \mathcal{L}_{\text{IPSD-}Tex}(\theta, \Delta V, S) = \mathbb{E}_{t, \epsilon} [w(t) (\epsilon_{ip}(z_{rgb,t}; y_1^{rgb}, \dots, y_{n_{ip}}^{rgb}, y_1^{txt}, \dots, y_{n_{ip}}^{txt}, t) - \epsilon) \frac{\partial z_{rgb}}{\partial \theta}], \quad (15)$$

$$\nabla_{\Delta V} \mathcal{L}_{\text{IPSD-}Tex}(\theta, \Delta V, S) = \mathbb{E}_{t, \epsilon} [w(t) (\epsilon_{ip}(z_{rgb,t}; y_1^{rgb}, \dots, y_{n_{ip}}^{rgb}, y_1^{txt}, \dots, y_{n_{ip}}^{txt}, t) - \epsilon) \frac{\partial z_{rgb}}{\partial \Delta V}], \quad (16)$$

$$\nabla_S \mathcal{L}_{\text{IPSD-}Tex}(\theta, \Delta V, S) = \mathbb{E}_{t, \epsilon} [w(t) (\epsilon_{ip}(z_{rgb,t}; y_1^{rgb}, \dots, y_{n_{ip}}^{rgb}, y_1^{txt}, \dots, y_{n_{ip}}^{txt}, t) - \epsilon) \frac{\partial z_{rgb}}{\partial S}]. \quad (17)$$

After initially localizing the partial image prompts onto the 3D object, it is then necessary to further optimize the texture of the 3D object globally. We further extend the IPSD losses in the texture optimization stage, using the multiple image prompt features to simultaneously optimize the 3D object:

$$f_{global} = \text{concat}(y_1^{rgb}, \dots, y_{n_{ip}}^{rgb}, y_{rgb} + \delta_{geo}), \quad (18)$$

$$\nabla_{\theta} \mathcal{L}_{\text{IPSD-}Tex}(\theta, \Delta V, S) = \mathbb{E}_{t, \epsilon} [w(t) (\epsilon_{ip}(z_{rgb,t}; f_{global}, t) - \epsilon) \frac{\partial z_{rgb}}{\partial \theta}], \quad (19)$$

$$\nabla_{\Delta V} \mathcal{L}_{\text{IPSD-}Tex}(\theta, \Delta V, S) = \mathbb{E}_{t, \epsilon} [w(t) (\epsilon_{ip}(z_{rgb,t}; f_{global}, t) - \epsilon) \frac{\partial z_{rgb}}{\partial \Delta V}], \quad (20)$$

$$\nabla_S \mathcal{L}_{\text{IPSD-}Tex}(\theta, \Delta V, S) = \mathbb{E}_{t, \epsilon} [w(t) (\epsilon_{ip}(z_{rgb,t}; f_{global}, t) - \epsilon) \frac{\partial z_{rgb}}{\partial S}]. \quad (21)$$

G Limitation and Discussion

Although IPDreamer proposed in this paper is capable of achieving high-quality 3D object texture editing, even when there is a significant discrepancy between the image prompt and the coarse NeRF model, the current image prompt adaptation cannot ensure the appearance of the generated result to be highly consistent with that of the given image prompt. In some cases, there are slight color differences between the generated 3D objects and the reference image prompts. Additionally, despite our method being faster than the text-to-3D method ProlificDreamer [74], further improvements in processing speed are required for practical deployment.

H Social Impact

Our IPDreamer does not have a direct negative impact on society. However, it is important to recognize the potential of high-quality 3D objects and ensure they are not adopted for malicious purposes.